J Indian Inst. Sci., Sept.–Oct. 1989, **69**, 381–408.

IISc THESES ABSTRACTS

Thesis Abstract (Ph.D.)

Molecular conformation and electronic structure of compounds related to amides and thioamides–A study by *ab initio* and semi-empirical molecular orbital methods by N. Ezhil.
Research supervisor: D. N. Sathyanarayana.
Department: Inorganic and Physical Chemistry.

1. Introduction

Recent progress in molecular orbital methods promises the potential for improving our understanding of the electronic structure and the role of various intramolecular forces governing the conformational stability[1]. The application of *ab initio* and semi-empirical molecular orbital methods is made presently to understand the molecular conformations and the electronic structure of a series of compounds closely related to amides and thioamides. The conformational isomerism of amides and thioamides is of paramount importance for understanding the factors which govern the conformations of peptides and proteins. These compounds also possess other biochemical and industrial importance[2,3]. The present work is seen as a logical extension of the previous proton and carbon-13 nuclear magnetic resonance and infrared and Raman spectroscopic studies including intramolecular potential field calculations carried out on these and other related molecules in this laboratory[3,4].

The compounds considered include,

1. Hydrazine carboxamides:

   $Y-NHC(=O)-Y_1$
   $Y = NH_2, \overset{+}{N}H_3$; $Y_1 = NH_2, NHNH_2, NH\overset{+}{N}H_3$.

2. Thiocarbamate esters

   $Y_1 \diagdown \atop Y_1 \diagup NC(=X)-Z$
   $Y, Y_1 = H, CH_3$; $X = O, S$; $Z = OCH_3, SCH_3$.

3 Biuret and diacetamide systems

   $Y-C(=X)-NHC(=X)-Y$
   $Y = NH_2, CH_3$; $X = O, S$.

4. Selenoamides and selenoureas and their thioanalogues.

   a. $Y-C(=X)-NY_1Y_1'$
   b. $YY'NC(=X)Y_1Y_1'$
   c. $Z-NHC(=X)-Z_1$

$Y, Y', Y_1, Y_1' = H, CH_3, NH_2$;
$Z, Z_1 = NH_2, NHNH_2$; $X = Se, S$.

The main objective of the molecular orbital calculations was to investigate the molecular conformations, their relative energies and electronic structure in a quantitative fashion and compare the results with experimental data. One of the most interesting features of conformational analysis is the study of internal rotations. Barrier-height measurements aid in understanding the forces giving rise to restricted rotation. The hindered internal rotation in amides has been the subject of many experimental and theoretical studies[5].

2. Experimental

The molecules investigated presently have two coupled rotational degrees of freedom. The appropriate potential surface has been obtained for these molecules employing the different m.o. methods. Because of the inherent limitations of these m.o. methods in predicting the stabilities of the different molecular conformations, several m.o. methods were presently utilised to note the consistency in the results. Hydrazine carboxamides show a change in the molecular conformation consequent to protonation. It was desirable to know the factors contributing to this conformational change and note how the electronic structure varies consequent to variation in the molecular conformation and as a result of protonation. N-protonated molecules play a vital role as intermediates in many organic reactions. Further, a study of the electronic structure of N-protonated compounds is important in the discussion of many biological problems[3].

Another important tool for the study of molecular structure is the concept of molecular electrostatic potentials[6]. The electrostatic potentials were calculated presently from the *ab initio* m.o. wave functions of the isolated molecule. The interaction energy of the molecule with the approaching electrophilic reagent is obtained. The calculations were performed in different planes. The results are correlated with the electronic structure.

The Fourier decomposition of the potential energy terms[7] has given some insight into the nature of the interactions involved in the rotation of methyl group over C-S/O bond. The separation of the total energy into various components involving the dipolar, back-bonding and steric considerations facilitates the interpretation. Thiocarbamate esters were subjected to such a study.

The structural and spectroscopic studies on selenium analogues of amides and ureas are meagre. The electronic structure of the corresponding sulfur and selenium compounds is expected to be very similar[8]. However, selenium in selenoamides and selenoureas may introduce steric and electronic effects, the selenium atom being more polarisable than sulfur. In this context, the m.o. calculations have been carried out. The CNDO/2 method was only employed since the other m.o. procedures are not adequately parametrised to include selenium.

A description of bonding in terms of computed bond orders and atomic charge densities is given. The variations in the electronic structure consequent to protonation, change in molecular conformation and the nature of the substituents are discussed. The computed potential barriers and overlap populations are correlated with the results of NMR and vibrational spectroscopic investigations.

References

1. PULLMAN, B. (ed.) *Quantum mechanics of molecular conformation*, Wiley, 1976.

2.	TRINCI, A. P. J. AND RYLEY, J F. (eds)	*Mode of action of antifungal agents*, Cambridge Univ. Press, 1984.
3.	BENEDETTI, E., DI BLASIO, B. AND BAINE, P.	*J. Chem. Soc. Perkin Trans. II*, 1980, 500–503.
4	DEVI, K R. G., MANOGARAN, S. AND SATHYANARAYANA, D. N.	*Phosphorus Sulfur*, 1981, **11**, 47–54.
5	PAYNE, P. W. AND ALLEN, L. C.	*Applications of electronic structure theory*, Schaefer III (ed.), Plenum, 1977, Ch. 2.
6.	TOMASI, J.	*Chemical applications of atomic and molecular electrostatic potentials* (eds P. Politzer and D. G. Truhlar), Plenum, 1981.
7.	RADOM, L., HEHRE, W. J. AND POPLE, J. A.	*J. Am. Chem. Soc.*, 1972, **94**, 2371–2381.
8.	ANTHONI, U., BORCH, G., KLAEBOE, P. AND NIELSEN, P. H.	*Acta Chem. Scand.*, 1982, **36A**, 69–77.

Thesis Abstract (Ph.D.)

Photoelectrochemistry of polycrystalline $SrTiO_3$ and $BaTiO_3$ semiconductor electrodes
by L. Gomathi Devi.
Research supervisor: T. R. N. Kutty.
Department: Inorganic and Physical Chemistry.

1. Introduction

The conversion and storage of solar energy using semiconductor/electrolyte junction are based either on photoelectrochemical cells (PECs) which incorporate the bulk semiconductor electrodes[1] or on semiconductor fine powder photocatalysts. PECs can be used to induce energy-storing chemical reactions, wherein electron-hole pairs are first generated in the semiconductor by absorption of photons. They are separated by the field in a depletion layer at the interface and electrons or holes are injected into the electrolyte to drive the redox reactions. A semiconductor to suit such purposes should have a proper band gap to match the maximum in the solar spectral distribution curve which at the same time should not undergo photocorrosion. Though many semiconductors are suggested for this purpose, there are some drawbacks. The semiconductors whose band gap is < 2.5 eV will corrode and those materials having larger band gap cannot make proper use of most of the solar energy whose intensity falls rapidly at shorter wavelengths. The problem, therefore, is either to improve the efficiency of the larger band-gap materials or to avoid corrosion of small band-gap semiconductors with suitable protective films. However, it is noticed that these protective films have deleterious effects on the efficiency of PECs due to large ohmic potential drop at the interface. Therefore, the present research is aimed at understanding the interfacial compositional variations of wide band-gap photoanodes (Perovskite titanates, $MTiO_3$). The results point to newer lines of approach with respect to defect states, crystallochemical relations to visible response and electrode surface treatments.

2. Preparation and characterisation

The titanates are prepared by either ceramic or chemical method. These methods are standardised for the preparation of high-purity powders of $MTiO_3$(M = Ba, Sr, Ca, Pb), their solid solutions as well as

those with the corresponding zirconates and the donor-doped phases through the oxalate precursor route[2]. The homogeneous precipitates are calcined to final product. The methods adopted for characterisation include X-ray powder diffraction, EPR, SEM and XPS as well as the electrochemical techniques. The steps involved in sintering the ceramics and their microstructural analysis are studied. Instrumental techniques used for photoelectrochemical measurements involve cyclic voltammetry current-voltage and capacitance measurements.

3. Results and discussion

The photoelectrochemical properties of polycrystalline $BaTiO_3$, $SrTiO_3$ and their solid solutions are studied. Many new features in the cyclic voltammograms, related to the surface states, are observed for the mechanically polished electrodes in the dark. These include the maxima in the anodic as well as the cathodic directions of the sweep and the abrupt rise in anodic current above ~ 0.5 V (SCE). These features in the cyclic voltammograms are not observed when the electrodes are etched in dilute acids for extended period of time. The nature of the surface states is investigated by alternating the etching and polishing of the same electrode, by varying the applied potential limits, change of pH, and concentration of alkali, the effect of dissolved H_2O_2 and O_2, modifying the electrode surface by applying Ti(III) and Ti(IV) solution and lastly, by reannealing the electrodes in oxidising as well as reducing atmospheres. The results show that the anodic maxima originate from the oxygen vacancies at the electrode surface where the strongly chemisorbed surface hydroxyls are present. Under the applied anodic potential and the accompanying upward band bending, electrons are transferred to the conduction band so that OH° radicals are formed. Interaction of these radicals with OH^- ions in the electrolyte produces peroxohydroxyls, HOO^-, which decompose to O_2 and H_2O under anodic potentials 0.5 V (SCE). The accompanying electron tunneling from the surface states to the conduction band, through the depletion layer, causes sudden rise in anodic current. The surface states which give rise to the cathodic peaks are related to dissolved O_2, since they vanish after the removal of O_2 in the electrolyte and also by limiting the upper voltage. They originate from surface hydroxyls attached to Ti^{4+} ions and facilitate the transfer of electrons to dissolved O_2 under cathodic potentials. The results show that these surface states themselves may act as electron traps leading to the formation of $Ti^{3+} - OH^-$ sites at the surface. The latter is involved in the H_2-evolution reaction at more cathodic potentials because the redox potentials of Ti^{3+}/Ti^{4+} and H_2/H^+ couples overlap. The easy formation of $Ti^{3+} - OH^-$ around the electron-rich $Ti^{3+} - V_O$ defect sites accounts for the enhanced intensity of the cathodic peaks on the etched surfaces and these maxima shift to the cathodic direction, with increasing applied potential limits.

I-V measurements are carried out at nearly steady-state conditions during band-gap illumination and using 1M NaOH as the electrolyte for polycrystalline electrodes, *viz.*, $BaTiO_3$:0.3% La, $BaTiO_3 - H_2$, $SrTiO_3 - H_2$ and $Sr_xM_{1-x}TiO_3$ (where M = Ba, Pb, Ca, etc.) solid solutions. The V_{On} potentials, where the photocurrents start appearing and are approximated to V_{fb}, are determined for the $I_p^2 vs\ V_{appl}$ curves following Gärtner relations. These plots are not linear throughout the range of applied potentials and differ considerably with the surface treatments.

Capacitance-voltage relations are measured for the semiconductor/electrolyte interface and from Mott-Schottky plots, the values of flat-band potential V_{fb} and donor density N_D at the space-charge layer are determined.

Dependence of photocurrent on wavelength has shown that the response of $BaTiO_3 - H_2$, $BaTiO_3$:0.3 La, and the other solid solutions having tetragonal phase tails into the visible region although the magnitude of photocurrents in the visible is much lower than those under band-gap illumination. The visible response for the materials having tetragonal phase is unaffected by chemical

etching as well as mechanical polishing. $SrTiO_3$ and other solid solutions having cubic phase shows low photoresponse to visible light only on polishing and is destroyed by chemical etching. The visible photoresponse arises from the mid band-gap states. The plots of $(\eta h\nu)^{\frac{1}{2}}$ *vs* $h\nu$ show that these mid-band-gap states extend to ~ 0.8 eV above the valence band edge for $BaTiO_3$. The variations in photocurrents with applied voltages and intensities of illumination showed that the visible light response is not a surface phenomenon but a bulk process occurring throughout the depletion layer. The hole-diffusion length (L_p) and the donor concentration in the depletion layer are obtained from the plots of $\ln(1-\eta)$ *vs* $(V - V_{fb})^{\frac{1}{2}}$. The polished electrodes show lower L_p and enhanced N_D values as compared to the corresponding etched electrodes under band-gap illumination.

The visible response of $BaTiO_3$ compared to $SrTiO_3$ can be explained on the basis of the difference in lattice defects[3]. $BaTiO_3$ has $V_{fb} = -0.9$ V and $V'_{fb} = 0.57$ V, so the mid-band-gap state is of 0.33 V ($= V'_{fb} - V_{fb}$). The defect states located ~ 0.3 eV below E_F may arise from Ti^{3+}–V_O centres whose EPR signal is detected both in $BaTiO_3$:La and $BaTiO_3 - H_2$. Mechanical polishing may introduce additional mid-band-gap states through the surface damage or lattice distortions around the surface region. This leads to the photoresponse in the visible spectrum for polished $SrTiO_3$ and the response vanishes on chemical etching[4]. The results indicate that the difference in photoelectrochemical characterisation for the tetragonal as compared to the cubic phase of the titanate and their solid solutions arise from the nature of the lattice defects which give rise to the mid-band-gap studies.

The kinetics of evolution of gaseous products H_2 and O_2 from the electrochemical cells having $SrTiO_3$ and $BaTiO_3$ photoanode is studied from the point of view of enhancing the efficiency of product generation. The rate of evolution of gases is less for polished electrodes compared to the etched ones. With increase in applied potential, the rate of evolution of the products increases and remains linear up to ~ 2 V (SCE), and at higher values the rate of evolution decreases, possibly due to irreversible changes in surface compositions. The rate of evolution increases with the concentration of alkali, in the range of 1–20 M NaOH.

Enhanced photoresponse is noticed for the titanate electrodes when exposed to dilute 1N NHO_3 + 0.05 M HF for extended periods up to 120 minutes. The steep rise in photocurrent at potentials just above V_{On} may indicate the elimination of surface recombination centres. The effects of concentration-temperature and time shows critical values and that the V_{On} potential shifts cathodically with the time of exposure to the reagent.

X-ray photoelectron spectra (XPS) of the variously treated electrode surface have been studied. The spectra show that the intensity ratio, N_O/N_{Ti}, decreases with the extent of reduction and the values are lower for mechanically polished samples as compared to those of the as-prepared ones. The surface composition of 1N HNO_3-treated (60 min) electrodes shows heterogeneity by way of the presence of surface hydroxyls, multiple bands for ($Ti\,2P_{4,3/2}$) and variations in N_O/N_{Ti} and N_{Sr}/N_{Ti} ratios. In the case of electrode surfaces treated with 1N HNO_3 + 0.05 N HF the concentration of F^- ion is found inversely related to that of hydroxyl ions. The surface compositions show heterogeneity including N_F/N_{Ti} and N_{Sr}/N_{Ti} ratios. The sputter-etching experiments show that the penetration of F is ~ 50 Å below the electrode surface.

References

1. FUJISHIMA, A. AND HONDA, K. Electrochemical photolysis of water at a semiconductor electrode, *Nature*, 1972, **238**, 37–38.

2. GOPALAKRISHNAMURTHY, H. S., SUBBA RAO, M. AND KUTTY, T. R. N. Thermal decomposition of titanyl oxalate S-I, *J. Inorg. Nucl. Chem.*, 1975, **37**, 891–898.

3. KUTTY, T. R. N. AND GOMATHI DEVI, L. Photoelectrochemical properties of donor doped $BaTiO_3$ electrodes, *Mater. Res. Bull.*, 1985, **20**, 793–801.

4. CHANG, B. T., CAMPET, G., CLAVERIE, J., HAGENMULLER, P. AND GOODENOUGH, J. B. Sensitization of polycrystalline $SrTiO_3$ (IV) photoanodes by mechanical polishing, *J. Solid St. Chem.*, 1983, **49**, 242–255.

Thesis Abstract (Ph.D.)

Grain boundary layer dielectric ceramics based on donor-doped $BaTiO_3$ by P. Murugaraj.
Research supervisor: T. R. N. Kutty.
Department: Inorganic and Physical Chemistry.

1. Introduction

Barium titanate-based compositions find use in switching (in single crystal form) and non-switching (in polycrystalline ceramic form) device applications. Two examples of the latter case are positive temperature coefficient of resistance (PTCR) and grain boundary layer capacitance (GBLC) effects. Donor-doped $BaTiO_3$ shows *n*-type conductivity whose electrical resistivity increases with temperature around Curie point. This is known as the PTCR effect. The same sample, when processed under different set of conditions, becomes insulating and shows abnormally high capacitance ($\sim 0.1\,\mu F$). Obviously, any explanation put forward for PTCR effect should be extendable to explain the origin of GBLC property as well. The GBL dielectric materials permit large values of capacitance to be obtained in small volumes and can thus be used in miniature capacitors, particularly in multilayer structures. The present investigation has been aimed at understanding the origin of PTCR and the GBLC properties.

2. Experimental techniques

Barium titanate with low-background impurities (Mn < 0.1, Fe $< 1.0\,\mu g/g$) is prepared from the successive precipitation of the precursor oxalate, $BaTiO(C_2O_4)_2 \cdot 4H_2O$. $BaTiO_3$:La or Nd (0.05 to 5.5 at.%) is prepared by coprecipitation with the precursor and the resulting product is adjusted with TiO_2 such that the final composition is $(Ba_{1-x}La_x)TiO_3$. Doping of transition metal ions (Mn or Fe) is carried out in solution and the amount incorporated in the precipitate (< 0.01 at.%) is determined by the atomic absorption spectrophotometry or quantitative EPR using MgO:Mn as the internal standard. Discs of 10 mm dia and 1 mm thick are sintered in air for 3–10 hours at 1650 K and cooled in a controlled manner (10–100 K h^{-1}). The average grain size decreased from 25 μm for pure $BaTiO_3$ to $< 2\,\mu m$ with donor content. Grain growth could be controlled by slow heating under oxygen partial pressure $< 10^{-5}$ atm. in donor-doped $BaTiO_3$. The sinter densities are around 95–97%.

In order to study the paramagnetic defect centres, EPR studies were carried out on a Varian E109 X-band spectrometer in the temperature range of 78–525 K. Structural studies were carried out using X-ray powder diffraction techniques with Philips PW 1050/70/76 X-ray diffractometer. Microstructural studies were carried out using scanning electron microscope manufactured by Cambridge Stereoscan (model S-150). Electron diffraction studies were carried out using transmission electron microscope (Philips EM301 model). In order to obtain the heat change across the phase transition in $BaTiO_3$, differential scanning calorimetry measurements were made using Dupont model 990.

Ohmic contacts for the ceramic discs are obtained by electroless nickel plating. dc resistivity of the sample is measured by the two probe technique. A constant voltage (0.01 to 0.1 V/cm) is applied to the test specimen and the current passing through it is measured. The capacitance and loss-tangent measurements were made with a bridge having separate oscillator and detector, the field applied being ~8 V/mm.

3. Results and discussion

EPR spectra of donor-doped $BaTiO_3$ exhibiting PTCR, show a weak signal with $g = 1.997$ in the tetragonal phase which acquires high intensity above the Curie point (398 K). The intensity of $g = 1.997$ signal is high for PTCR samples when compared to that of H_2-N_2-annealed $BaTiO_3$. This signal is identified to arise from singly ionised Ba-vacancies (V'_{Ba}). Higher concentration of Ba-vacancies is formed in donor-doped samples arising from the mixed compensation mechanism, namely, conduction electron as well as cation vacancy compensation. In the tetragonal phase, Ba-vacancies are either neutral (V_{Ba}) or doubly ionised (V''_{Ba}, He-like) and hence do not show any EPR signal. In the cubic phase, they are singly ionised. If V''_{Ba} were present in tetragonal phase, $V''_{Ba} \rightleftharpoons V_{Ba} + e'$ conversion across the phase transition should lead to enhancement in conductivity. Since reverse is the case, V_{Ba} should be the predominant defect in the tetragonal phase and converts to V'_{Ba} in the cubic phase. Thus the activation of these centres leads to the trapping of charge carriers which are not available for conduction and hence the increase in electrical resistivity. The $g = 1.997$ signal is weak in single crystals when compared to that of ceramic samples (La < 0.4 at.%). The signal intensity decreases with grain size *i.e.*, decreasing contribution from grain boundary layers. The signal intensity is also affected by the sintering and cooling conditions as well as addition of extra TiO_2 as a sintering aid. These observations are explained on the basis of higher concentrations of V'_{Ba} at the grain boundary layer than in the bulk of the grain. This conclusion is in agreement with the kinetic studies on the defect chemistry of $BaTiO_3$ reported by Wernicke[1] and Daniels *et al*[2]. In donor-doped samples, the concentration of Ba-vacancies is enhanced through vacancy compensation. The diffusion coefficient of V_{Ba} is many orders of magnitude smaller than that of V_O. At practical cooling rates necessary to generate PTCR effect Ba-vacancies lag behind the O-vacancies and retain higher concentrations near grain boundaries than in the bulk. Thus the polycrystalline ceramic sample shows pronounced PTCR effect when compared to single crystals.

Mn at low concentrations (< 0.1 at.%) is found to enhance the PTCR effect in $BaTiO_3$:La ceramic. PTCR $BaTiO_3$, doped with 0.01–0.02 at.% Mn does not show any EPR signal arising from Mn in tetragonal phase whereas Mn^{2+} signal is observed for the same sample in the cubic phase as well as in rhombohedral phase. Mn can exist in oxidation states other than 2+ in tetragonal and orthorhombic phases. Mn^{3+} with short relaxation time is observed only below 4.2 K. If Mn is present in tetragonal phase as Mn^{4+}, its signal should appear since Mn^{4+} is found to have larger relaxation time in $SrTiO_3$, TiO_2, etc. Hence the absence of Mn signals can be attributed to the presence of Mn in 3+ state which converts to Mn^{2+} above 400 K. This is explainable on the basis of $Mn^{3+} + e' \rightleftharpoons Mn^{2+}$ conversion across the phase transition. Thus Mn^{3+} acts as a trap centre for charge carriers and enhances the PTCR by augmenting the action of V_{Ba}.

Fe^{3+} (< 0.1 at.%) impurity also is found to enhance the PTCR effect. The defect centre responsible for this is identified to be $Fe^{3+} - V_O$ complex giving rise to an EPR signal with $g_\parallel = 5.543$ and $g_\perp = 11.831$. These signals are observed at 300 K and they disappear just before the Curie temperature. These observations are explained on the basis of $Fe^{3+} - V_O$ trapping a conduction electron and becoming $Fe^{4+} - V_O(e')$ which will have even spin state and will not be observable by EPR[3].

The above explanation is further supported by the observations on donor-doped $SrTiO_3$ (cubic at

300 K). The resistivity of La-doped $SrTiO_3$ sintered in air is very high when compared to $BaTiO_3$:La samples. EPR signals arising from $V_O^{\cdot}$ and Mn^{2+} can be observed at 300 K which is in agreement with the result from cubic $BaTiO_3$. Mn^{4+} signal ($g_{av.} = 1.997$) is observed in oxygen-annealed $SrTiO_3$:La ceramics, while the same sample shows Mn^{2+} ($g = 2.004$) and $Mn^{2+} - V_O$ ($g = 2.0001$) signals when annealed at low p_{O_2} ($< 10^{-5}$ atm.). Mn^{2+} intensity decreases continuously with temperature and vanishes at ~ 160 K (T_c). The activation energy is found to be 0.065 eV which corresponds to one of the TO soft modes of $SrTiO_3$[4].

These observations show that the charge redistribution at the corresponding acceptor states leads to changes in resistivity around the phase transition. These observations also indicate that the charge redistribution among the acceptor levels arises from the interaction of electronic states with the soft phonon modes under extrinsic conditions.

The PTCR ceramic, when cooled slowly (10 K h^{-1}) from the sintering temperature, becomes insulating and shows effective dielectric constant $> 10^5$. As already seen, Ba-vacancies are formed at the grain boundaries and diffuse into the bulk. During cooling, the diffusion front advances and gets frozen below 1400 K. This ceramic will have a heterogeneous distribution of defects. It has highly insulating grain boundaries and conducting grain cores. The ceramic can be considered to constitute thin dielectric grain-boundary layers enveloping the conducting grain cores. As a result, the specimen can be regarded in terms of an equivalent circuit of hundreds of microcapacitors connected in series (fig. 1)[5]. The variations in EPR signals with Nd content, indicate that a certain fraction of the donor-doped $BaTiO_3$ is cubic even at 300 K. The X-ray powder diffraction data support the EPR results. The effect of grain size variation on EPR signal intensity indicates that the boundary layers surrounding the grain may constitute the cubic phase. Higher concentration of Ba-vacancy may be the cause for the stabilisation of cubic phase. Since the acceptor states arising from the Ba-vacancies and the impurities are activated in the cubic phase, the laser is electrically more insulating than the semiconducting tetragonal interiors. The cubic grain-boundary layer acts as effective dielectric media where the field tends to concentrate. As a result, the abnormal dielectric constant is observed in these ceramics.

X-ray and EPR results on $BaTiO_3$:Nd ceramics (Nd < 5.5 at.%), show the coexistence of paraelectric cubic along with the ferroelectric tetragonal and orthorhombic phases over a wide range of temperature and composition. Dielectric peak around the phase-transition temperature is broad and shifts to lower temperatures with Nd content in these ceramics. The heat of transformation measured at the Curie point tends to zero above 3.5 at.% Nd and the phase transition approaches that of second order. These are characteristics of diffuse phase transition occurring in this system. The Curie temperature of the bulk decreases with increase in Nd content. Quantitative values of these phase fractions of $BaTiO_3$ are obtained from EPR and X-ray diffraction measurements. A T-x topological diagram is presented for $BaTiO_3$:xNd system ($x < 5.5$ at.%). The phase contents are found to vary with processing parameters as well as grain size and the very existence of more than one phase in a given area of the phase diagram indicates the thermodynamic equilibrium prevailing in $BaTiO_3$:Nd ceramics[6]. The inhomogeneous distribution of lattice defects may be the major cause for such a behaviour.

At higher Nd concentration (> 5.5 at.%), X-ray and electron diffraction studies show that phases amorphous to X-rays are formed. Two types of phases (high Nd-containing $BaTiO_3$ and Ba-containing $Nd_2Ti_2O_7$) are identified. Fraction of the X-ray amorphous phases increases with Nd content. In the range $0.15 < x < 0.3$, the ceramic can be considered to constitute Nd-doped $BaTiO_3$ grains with amorphous $(Nd, Ba)_2Ti_2O_7$ phase dispersed at random. Due to the existence of such a heterogenity, the ceramic shows $\varepsilon_{eff} > 10^4$. A relaxation behaviour is observed in these ceramics at low frequencies. This phenomenon is explained as due to the Maxwell-Wagner type of interfacial

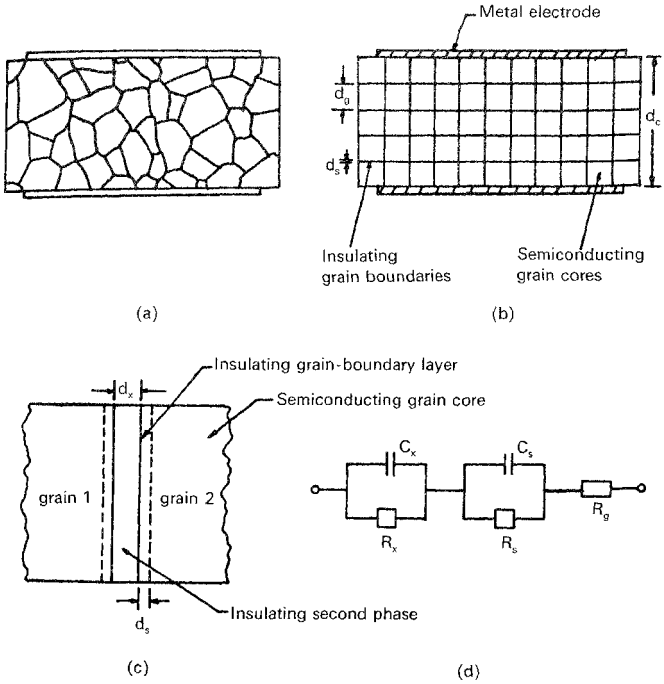

FIG. 1. Conceptual description of grain-boundary layer capacitor: (a) hypothetical representation of a grain-boundary layer capacitor disc; (b) conceptual microstructure; (c) structure of a grain boundary, and (d) equivalent circuit for a grain boundary.

relaxation polarisation arising from the heterogeneous nature of the system *i.e.*, due to the presence of secondary intergranular phases[7].

References

1. WERNICKE, R The influence of kinetic processes on the electrical conductivity of donor-doped $BaTiO_3$, *Phys. Status Solidi*, 1978, **47(a)**, 139–144.

2 DANIELS, J AND WERNICKE, R	Defect chemistry and electrical conductivity of doped barium titanate ceramics, Part V. New aspects of an improved PTC model, *Philips Res. Rep.*, 1976, **31**, 544–559.
3 KUTTY, T R N., MURUGARAJ, P. AND GAJBHIYE, N. S.	EPR evidence for activation of trap centres in PTCR $BaTiO_3$ ceramics, *Mater. Res. Bull.*, 1985, **20**, 565–574.
4. KUTTY, T. R. N., GOMATHIDEVI, L. AND MURUGARAJ, P.	The change in oxidation state of Mn ions in semiconducting $BaTiO_3$ and $SrTiO_3$ around the phase transition temperatures, *Mater. Res Bull.*, 1986, **21**, 1093–1102.
5. MURUGARAJ, P. AND KUTTY, T R. N.	EPR studies on the donor doped $BaTiO_3$ grain-boundary layer dielectrics, *Mater. Res Bull.*, 1985, **20**, 1473–1482.
6. MURUGARAJ, P., KUTTY, T R N. AND SUBBARAO, M.	Diffuse phase transformations in Nd doped $BaTiO_3$ ceramics, *J. Mater. Sci.*, 1986, **21**, 3521–3527.
7. KUTTY, T. R N. AND MURUGARAJ, P.	Phase relations and dielectric properties of $BaTiO_3$ ceramics heavily substituted with Nd, *J. Mater. Sci.*, 1987, **22**, 3652–3664.

Thesis Abstract (Ph.D.)

Experimental studies on gas-microphone-detected photoacoustic signals from condensed phases by T. Somasundaram.
Research supervisor: P. Ganguly.
Department: Solid State and Structural Chemistry Unit.

1. Introduction

Gas-microphone-detected photoacoustic spectroscopy (PAS) has attained an important status as a tool for probing optical and thermal properties of materials[1,2]. The advantages of PAS are mainly the ease with which an ordinary optical spectrometer is modified to probe the material and the ease with which details are obtained through this technique from several samples having a variety of physical shapes and sizes[3]. Recent studies carried out in this laboratory have indicated the possibility of enhancing the PA signals by an order of magnitude and the possibility of recording spectra of materials under gas-flow conditions at elevated temperatures. The implications of these findings on the well-known theories of PA effect[1], the mechanism of the PA signal generation under these conditions and application of these studies are described below.

2. Experimental

An indigeneous PA spectrometer working in the UV-VIS range and capable of operating at ambient conditions of temperature and pressure has been fabricated. Sample cell which is the heart of the instrument has been built with care. Various sample cells for recording spectra of materials at high- and low-temperatures, variable gas lengths, changing gases and vapours, etc., have been designed and constructed. All these cells have been checked and calibrated for their optimum performance. Most of the samples used for the study are of AR grade and in certain cases materials have been prepared from AR chemicals by following standard procedures.

3. Results and discussion

Since the aim of the work described below is essentially the utilisation of the PA spectrometer for

studying different phenomena, the work carried out falls into different categories and hence they will be treated and discussed separately in the following sub-sections.

3.1. *Enhancement of PA signals*

The strength of the PA signal depends, apart from the optical characteristics of the sample, on the thermal characteristic of the coupling gas[4]. A few reports have appeared in literature on the enhancement of the PA signal by ~ 2.5 times[5,6]. This has been achieved by replacing air by helium (which has higher thermal diffusivity). Experiments carried out in this laboratory have indicated that introduction of certain volatile liquids (which by themselves do not absorb the light and hence do not generate the signal) into the cell without wetting the sample, can enhance the PA signals by as high as an order of magnitude[7]. Figure 1 shows the PA spectrum of a powdered solid $Nd_3Al_5O_{12}$ recorded in the presence of air and air + ether vapour mixture. The spectrum in the presence of ether is enhanced about seven times without any loss in the spectral information. Using this method spectra of solids (both in the powder and single crystal forms), liquids, coatings and biological matter have been recorded with increased signal strength. This procedure can, therefore, be used easily to improve the spectral quality in terms of resolution and signal strength.

The extent of enhancement (E) has been found to critically depend upon whether the sample is non-porous or porous in nature[8]. For non-porous materials, E is more for higher absorption coefficients. In general E is higher for higher vapour pressures. The mechanism of enhancement may be attributed to two different processes, *viz.*, either a more efficient heat transfer from the solid to the

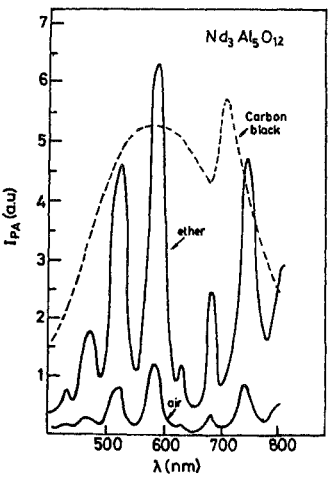

FIG. 1. Unnormalised PA spectrum of $Nd_3Al_5O_{12}$ in the presence of air and ether.

gas and/or to the desorption of the adsorbed vapour molecules into the gas phase. The PA signal arises due to the periodic diffusion of heat (generated following light absorption) into the gas[4]. The amount of heat extracted from the solid to the gas is therefore crucial. The amount of heat partitioned between the solid and the gas depends on the ratio of the square root of the thermal constants of the solid and the gas[2]. The ratio is more for the liquid-solid combination than the gas-solid combination. We believe therefore that the introduced vapour is likely to produce a liquid layer of optimum thickness so that more heat is extracted into the gas through the intervening liquid layer. To get higher E_r the layer should not also be very large as this will prevent heat going into the gas. The extracted heat can desorb some of the liquid molecules so that an additional thrust is given to the acoustic piston.

3.2. *Studies with an open PA cell*

There is a general belief that PA experiments have to be carried out in closed cells so that there is no heat loss from the cell or noise addition into the cell[1]. However, Dioszeghy *et al*[9] have shown that an open PA cell can be constructed without appreciable loss in signal. Our experiments have indicated that a truly open PA cell can be constructed without loss in signal even under flowing gas conditions[10,11]. Typical result is shown in fig. 2 where spectra of a catalyst Cr^{6+}/Al_2O_3 has been recorded at various temperatures when vapours of acetone are flowing through the cell. The important requirement for the cell to operate under these conditions is the dimension of the capillaries through which the gas is passed which has been maintained to be ~ 0.5 mm id. The frequency dependence of the signal changes for chopping frequencies < 15 Hz when the cell is open or when a gas is passing through the cell. Another interesting observation in the open cell is that except for carbon black all the other samples studied so far (which includes a wide variety of samples with diverse optical and thermal properties such as alumina catalyst, CdS single crystal, a-Se, $SrMoO_3$, etc.) do not

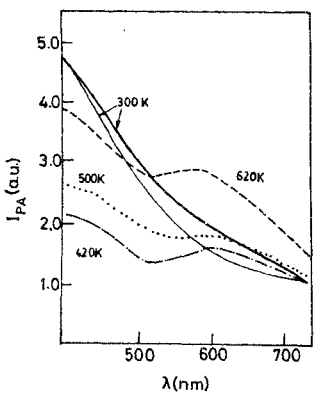

FIG. 2. Normalised PA spectra of chromia-alumina catalyst as a function of temperature in the open cell.

show any dependence of signal on flow rate. Carbon black alone shows a dependence; a decrease in signal with increase in flow rate. The other samples do not show a flow rate dependence even at high flow rates (ten times the volume of the cell displaced during a chopping period).

The mechanism of the signal generation in an open cell under gas-flow condition and the flow rate independence seen with almost all the samples except carbon black is not very clear. The difference in behaviour seen with carbon black cannot be attributed to its thermal or optical properties alone because wide variety of other materials differing in these properties do not show the dependence. One possibility is the porous nature of carbon black which can modify the thermal properties of a bulk material into a air + bulk composite which will be different from the bulk.

3.3. *Studies with powders*

PA spectroscopic studies carried out on powders such as a-Se, dye-adsorbed alumina catalyst, etc., have indicated that PA signal depends critically on the paticle size. A careful analysis indicated a new $(\text{delta})^{-1/2}$ dependence of PA signal, where (delta) is the particle size. Surface area of the catalyst does not influence the signal to a greater extent. In addition to these findings, the results of the dye-adsorbed catalysts have shown that there need not be a linear correlation between the amount of dye adsorbed and the signal intensity, especially in the high-concentration ranges.

3.4. *Phase-transition studies*

PA effect has been used to study several thermal phase transitions encountered in solids. The studies have been carried out on well-known samples such as $BaTiO_3$, $NaNO_2$, CoO, NH_4NO_3, VO_2, etc., in order to find out the exact correlation between the PA signal strength and the thermal properties of the samples. The experiments have been carried out on samples either directly or after mixing with small amounts of carbon black[12]. The results have indicated that the signal depends, to a certain extent, upon the specific heat of the material; however, the thermal diffusivity seems to be an important parameter. Some of the results like the independence of changes in signal both under saturated and unsaturated conditions and others have indicated the differences between the experimental observations and the theoretical predictions of PA effect. Some preliminary studies on the dehydration of metallic hydrates have also been carried out with the help of PA spectroscopy.

3.5. *Study of surfaces and biological matter*

The PA spectroscopic method of analysis is convenient to study the surface optical properties of materials due to its insensitiveness on the surface morphologies. Exploiting this advantage surface acidities of zeolites like ZSM-5, ZSM-11, ALPO-5 and SAPO-5 have been estimated quantitatively with the aid of aminetitration method and PA spectroscopy[13]. The estimated surface acidity correlates well with the ammonia thermal desorption data on these catalysts. The acidity distribution of various zeolites studied is shown in fig. 3.

Fungi which do not possess chlorophyll are generally colourless and are not candidates for a PA study. However, a class of fungi called thermophilic (heat-loving) fungi which grow and thrive only at high temperature conditions, have fascinating colours. For a particular fungus the colour changes with time, temperature and nature of the growing medium. PA spectroscopy came as a handy tool to study the nature of the pigments of the fungi since other conventional spectroscopic methods required the extracation of the pigment from the fungi. *In vivo* PA study, infrared spectra and chemical analysis of these fungi along with the easy transformation from one colour to another have indicated that aphins (pigments in the insects, aphids) can be one of the possible candidates for the pigments[14].

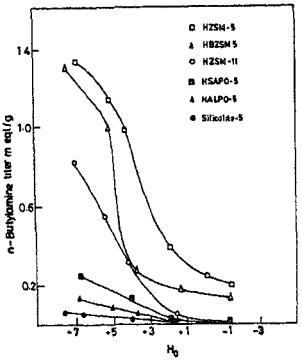

FIG. 3. Plot of *n*-butylamine titre value against Hammett acidity (H_0) for various zeolite samples.

4. Conclusions

The above studies clearly indicate the possible use of PA spectroscopic technique for the study of solids and surfaces. The enhancement of the signal can be used to study very small absorption coefficient materials, the open cell can be used to follow the mechnaism and product distribution of heterogeneous catalysts when the cell is appropriately coupled to a GC–MS, the studies with powders indicate the precaution one has to take before interpreting the results from powdered materials, the phase transition studies indicate the ease of following many phase transitions using a simple home-built PA spectrometer and finally the surface study indicates the importance of this method's surface-sensitive nature.

References

1. ROSENCWAIG, A. — *Photoacoustics and photoacoustic spectroscopy–Chemical analysis*, 1980, Vol. 57, Wiley.
2. TAM, A. C. — *Rev. Mod. Phys.*, 1986, **58**, 381–431.
3. GANGULY, P. AND RAO, C. N. R. — *Proc. Indian Acad Sci. (Chem. Sci.)*, 1981, **90**, 153–214.
4. ROSENCWAIG, A. AND GERSHO, A. — *J. Appl. Phys.*, 1976, **47**, 64–69.
5. WONG, K. Y. — *J. Appl. Phys.*, 1978, **49**, 3033–3035.
6. AAMODT, L. C., MURPHY, J. C. AND PARKER, J. G. — *J. Appl. Phys.*, 1977, **48**, 927–933.
7. GANGULY, P. AND SOMASUNDARAM, T. — *Appl. Phys. Lett.*, 1983, **43**, 160–162.
8. GANGULY, P. AND SOMASUNDARAM, T. — *Appl. Phys. B*, 1987, **43**, 43–52.

9. DIOSZEGHY, T., MIKLOS, A., KELEMEN, A. AND LORINCZ, A.	*J. Appl. Phys.*, 1985, **58**, 2105–2108.
10. GANGULY, P. AND SOMASUNDARAM, T.	*Proc Indian Acad. Sci. (Chem. Sci.)*, 1987, **98**, 305–309.
11. SOMASUNDARAM, T. AND GANGULY, P.	*Bull. Mater. Sci.*, 1987, **9**, 81–87.
12. SOMASUNDARAM, T., GANGULY, P. AND RAO, C. N. R.	*J. Phys. C. Solid St. Phys.*, 1986, **19**, 2137–2151.
13. SOMASUNDARAM, T., GANGULY, P. AND RAO, C. N. R.	*Zeolites*, 1987, **7**, 404–407.
14. SOMASUNDARAM, T., RAO, S. S. R. AND MAHESHWARI, R.	*Curr. Sci.*, 1986, **55**, 957–960.

Thesis Abstract (Ph.D.)

X-ray crystallographic investigations on metal complexes of nucleic-acid constituents by Noor Shahina Begum.
Research supervisor: H. Manohar.
Department: Inorganic and Physical Chemistry.

1. Introduction

Metal ions are essential for a large variety of biological processes in general and have an important role specifically in the biochemistry of nucleic acids. Binding studies of metal ions to nucleic-acid derivatives are currently of great interest especially in view of the speculation that antitumour Pt drugs may act by crosslinking DNA. Nucleotides, which are the building blocks of nucleic acids, have multiligating sites and thus can coordinate to metal ions in a variety of ways. In addition, it has been shown[1] that interligand interactions between chelate ligands and nucleic-acid derivatives in the primary coordination sphere influence the stereoselectivity of binding of metal complexes to nucleic-acid constituents. Further, the ternary metal-nucleotide complexes containing heterocyclic amines are of special interest for the reason that they can be regarded as simple models for the naturally occurring substrate metal ion-aromatic amino-acid centres found in proteins. The present study is concerned with the syntheses and X-ray structural studies on ternary metal complexes with both ribo- and deoxyribonucleotides and aims at understanding the influence of the ternary ligands such as ethylenediamine (en), imidazole (im) and benzimidazole (bim) on the coordination behaviour of nucleotides. All the structures were solved by Patterson and Fourier techniques and refined by least-squares method.

2. Experimental

The structures of the ternary Co(III)ethylenediamine complexes with 5′-IMP and 5′-GMP have been solved earlier in our laboratory[2]. This study has been extended to the Ni(II) complexes with 5′-GMP and 5′-dGMP, $[Ni(5'\text{-dGMP})_2(en)_{0.7}(H_2O)_{0.6}(H_2O)_2]^{2-}$ $[Ni(en)_{1.3}(H_2O)_{1.4}(H_2O)_2]^{2+}\cdot 7H_2O$ (1) and $[Ni(5'\text{-GMP})_2(H_2O)_4]^{2-}$ $[Ni(en)_2(H_2O)_2]^{2+}\cdot 6H_2O$ (2). The two structures are essentially isostructural, except for the nature of en coordination in (1). An interesting feature of the structure of

(2) is that the ternary ligand, en and the nucleotide moieties are not coordinated to the same metal ion. One of the metal ions, Ni(1), lying on a crystallographic two-fold axis parallel to *b* is octahedrally coordinated by two N(7) atoms of the symmetry-related oxopurine nucleotides in *cis* position and four water molecules. The metal ion Ni(2) lies on another two-fold axis parallel to *a* and is octahedrally coordinated by two bidentate en and two water molecules. In compound (1), on the other hand, en coordinates both at Ni(1) and Ni(2) with partial occupancies. The nucleotide conformations in both complexes are C(2')-*endo*, *anti*, *gg*. The *cis*-binding of nucleotides in the present structure is similar to that observed for the intrastrand crosslinking models proposed to explain the antitumour activity of *cis*- $[Pt(NH_3)_2Cl_2]$.

In the structure[3] of $[Cu(bim)(H_2O)_5]^{2+}[5'\text{-IMP}]^{2-}\cdot 3H_2O$, the octahedral coordination around Cu has nitrogen of bim ligand and five water molecules. The nucleotide is held by stacking and hydrogen-bonding interactions only. The nucleotide conformation is defined by C(3')-*endo*, *anti*, *gg*. This structure is the first example of the absence of direct metal-nucleotide interaction.

Ribose coordination is observed for the first time in the structure of $[Cu(im)_2(5'\text{-UMP})(H_2O)]\cdot 5H_2O$. Interestingly, the two molecules in the asymmetric unit have different coordination geometries for Cu(II), one being trigonal-bipyramidal and the other square-pyramidal geometry. The five coordination sites are defined by the two oxygens of ribose hydroxyls, two im ring nitrogens and a water oxygen. The nucleotide conformation of both the moieties is defined as C(2')-*endo*, *anti*, *gg*.

$[Cu(bim)(5'\text{-dGMP})(H_2O)_3]\cdot 4H_2O$ is the second example of a ternary complex of a deoxynucleotide. This structure has two molecules in the asymmetric unit with Cu(II) of both the molecules showing square-pyramidal coordination. 5'-dGMP coordinates through N(7) atom of the base, which is very unusual for a metal nucleotide complex containing a π-aromatic amine. A feature of particular interest is the unusual sugar conformation. The furanose ring of one molecule adopts C(3')-*exo*/C(2')-*endo* pucker and that of the other adopts C(3')-*exo* pucker. The conformation about C(4')-C(5') bond is *gg*. The nucleobase is in the *anti* orientation with respect to the sugar.

The crystals of the binary complex $[Cu(theo)_2(H_2O)_3]\cdot 2H_2O$ are reflection twins about (001) face. The structure was solved to a final *R* value of 0.069. Cu(II) has a (4 + 1 + 1) distorted octahedral coordination geometry, with two theophylline (theo) molecules and two water molecules at equatorial sites and another water molecule at axial position. The remaining apical position is occupied by exocyclic oxygen O(6) at a longer distance. This structure is one of the rare examples where N(7)/O(6) chelation mode of binding is observed.

This study reveals the subtle variation in the coordination behaviour of the nucleotide in presence of the π-aromatic amines. In contrast to the observations made from solution studies which reveal phosphate binding of nucleotides, we have obtained crystallographic evidence of stacking interactions, sugar binding and also base binding in complexes containing im and bim as ternary ligands in preference to phosphate binding.

References

1. MARZILLI, L. G. AND KISTENMACHER, T. J. — *Acc. Chem. Res.*, 1977, **10**, 146–152.
2. POOJARY, M. D. AND MANOHAR, H. — *J. Chem. Soc. Chem. Commun.*, 1982, 533–534.
3. POOJARY, M. D., SHAHINA BEGUM, N, MANOHAR, H. AND BAU, R. — *J. Chem. Soc. Chem. Commun.*, 1985, 821–822.

Thesis Abstract (Ph.D.)

Carbon, oxygen and nitrogen (six-membered ring) annulations by Vilsmeier reaction by M. Sreenivasulu.
Research supervisor: G. S. Krishna Rao.
Department: Organic Chemistry.

1. Introduction

The construction of substituted benzenes is an important synthetic objective of organic chemists. Ring functionalisation is not the only approach that can be envisaged, since it is also possible to construct the ring with some or all of the substituents already in position starting from suitable acyclic precursors. A major advantage with the benzoannulation technique is that it can be used to prepare aromatic compounds with substitution patterns not easily attained by conventional synthesis. One of the recent developments in this area is the use of Vilsmeier reaction[1] to synthesise a great variety of aromatics and heteroaromatics from acyclic precursors in a simple manner. It is based on an electrocyclic (thermal) hexatriene-cyclohexadiene ring closure combined with an elimination reaction. Annulation by Vilsmeier reaction route, involving the use of simple and easily accessible starting materials, constitutes the theme of the thesis.

2. Experimental

2.1. *Benzenemono-, di- and tricarboxaldehydes*

A one-step, simple convenient synthesis of various substituted benzenemono-, di-, and tricarboxaldehydes from β,γ-unsaturated alkenols (**1**) has been developed using the Vilsmeier reaction[2–4]. The β,γ-unsaturated alkenols were prepared from aldehydes, ketones and acids. The study shows that iminoalkylate intermediate of a suitably substituted alkenol initiates subsequent cyclisation. At least five contiguous carbon atoms are found essential for benzocyclisation to occur. The Vilsmeier reaction on three structurally different β,γ-unsaturated alkenols demonstrates its mechanistic uniqueness in producing an identical end-product, *viz.*, uvitaldehyde (**2**). Uvitaldehyde has been used as a synthon in the synthesis of a naturally occurring alkaloid, hydroechinuline[5]. Alkyl substituents at 1 and 3 or 1 and 5 or 3 and 5 positions of the starting pentenol gave dialkyl-substituted monoformylbenzene. Increase in the number of substituents drastically reduces the yield of the product. The di- and tricarboxaldehydes synthesised by this one-step route are not readily accessible by other routes.

2.2. *Chlorobenzenemono-, di- and tricarboxaldehydes*

Vilsmeier reaction on ketones has been well studied, but only a few reports are available on the use of alkenones as substrates. This led to the present study of the Vilsmeier reaction on α,β-unsaturated alkenones (**3**), prepared by the action of alkyllithium on the appropriate acids. Chlorobenzenemono-, di- and tricarboxaldehydes (**4**) were synthesised in one-step from substituted pentenones. The incorporation of chlorobenzenecarboxaldehyde moiety in natural products like ascochlorin and collectochlorin-A[6] is of significance. Since established procedures are available to manipulate –cl and –CHO groups to other functionalities, the amenability of polyformylchlorobenzenes obtained in this study for elaboration to other synthetically useful benzenoids would be of considerable synthetic value.

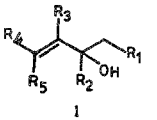

I

e.g., $R_1 = R_2 = R_4 = H$; $R_3 = R_5 = CH_3$

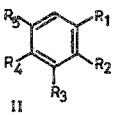

II

$R_1 = R_5 = CHO$; $R_2 = R_4 = H$; $R_3 = CH_3$

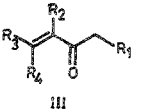

III

e.g., $R_1 = R_3 = H$; $R_2 = R_4 = CH_3$

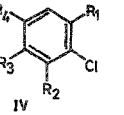

IV

$R_3 = H$; $R_4 = R_1 = CHO$ $R_2 = CH_3$

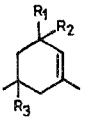

V $R_1, R_2 = O$; $R_3 = H$

VI $R_1, R_2 = O$; $R_3 = CH_3$

VII $R_1, R_2 =$  ; $R_3 = CH_3$

VIII

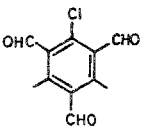

IX

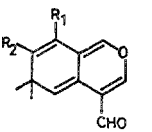

X $R_1 = Cl$; $R_2 = H$

XI $R_1 = Cl$; $R_2 = CHO$

XII $R_1 = H$; $R_2 = CHO$

XIII

e.g., $R_1 = CH_3$; $R_2 = CH_2CH_3$

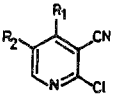

XIV

$R_2 = R_1 = CH_3$

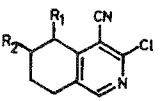

XV

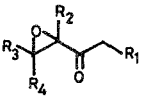

XVI

e.g., $R_1 = R_2 = H$; $R_3 = R_4 = CH_3$

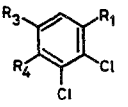

XVII

$R_1 = CHO$; $R_3 = H$; $R_4 = CH_3$

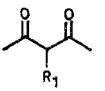

XVIII $R_1 = H$

XIX $R_1 =$ Phenyl

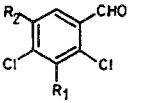

XX $R_1 = R_2 = H$

XXI $R_1 = H$; $R_2 = CHO$

XXII $R_1 =$ Phenyl ; $R_2 = H$

2.3. *Benzopyrans*

Monocyclic pyrones were obtained from various simple ketones by Vilsmeier formylation. Earlier Traas and coworkers[7] isolated a benzopyran derivative from Vilsmeier reaction on isophorone. Similar pyran annulations in related systems have been observed in the present study. Thus compounds (**6** and **8**) related to isophorone (**5**) undergo hetero(oxygen)annulation in one-step to give the benzopyran derivatives (**9**–**11**). The structures of the benzopyrans (**9** and **10**) were confirmed by X-ray studies. The most important step in the proposed mechanism is the electrocyclic 6π-dienal-α-pyran ring closure. In contrast, 3,5-dimethyl-2-cyclohexenone (**7**) gave only the hexasubstituted chlorobenzenecarboxaldehyde (**12**). Treatment of **9** with conc. sulfuric acid led to methyl migration and aromatisation, the plausible structure of the product being 8-chloro-6,7-dimethyl-1H-2-benzopyran-4-carboxaldehyde (**13**). The 7-substituted benzopyrans **10** and **11**, on the other hand, did not undergo methyl migration on similar acid treatment, instead the unchanged starting materials were recovered.

2.4. *o-Dichlorobenzenecarboxaldehydes*

o-Dichloroaromatic compounds find diverse applications, for example, as starting materials for the synthesis of natural products and physiologically active compounds[8]. The Vilsmeier reaction of α,β-epoxy ketones, so far not known, has been studied. The α,β-epoxy ketones (**14**) are readily accessible from the corresponding α,β-unsaturated ketones by treatment with alkaline hydrogen peroxide. The novel, single-step synthesis of *o*-dichlorobenzenecarboxaldehydes obtained by the Vilsmeier route from acyclic α,β-epoxy ketones is interesting and versatile. The procedure brings about three operations in a single step: benzoannulation, introduction of two chlorine atoms in the *ortho* position and formylation. The study has been extended to cyclic epoxy ketones (**15**) which gave monochlorobenzenoids and *o*-dichlorobenzenoids. The formation of monochlorobenzenoids from cyclic epoxy ketones was rationalised on the basis of elimination of HCl during aromatisation.

2.5. *2-Chloronicotinonitriles and fused 2-chloro-3-cyanopyridines*

Substituted 2-chloronicotinonitriles are of medicinal and synthetic importance[9]. A new, convenient single-step method for the synthesis of mono- and disubstituted 2-chloronicotinonitriles[10] (**18**) has been developed by the Vilsmeier reaction on alkylidenemalononitriles (**17**). The alkylidenemalononitriles were prepared by the Knoevenagel condensation[11] of aldehydes or ketones with malononitrile. The malononitriles from cyclic ketones also underwent similar pyridoannulations to give fused 2-chloronicotinonitriles (**19**). The malononitrile derived from 6-methoxy tetralone afforded benz(f)isoquinoline. Regiospecific formation of the products were observed. The present one-step procedure of pyridoannulation leading to chloronicotinonitriles has considerable potential in the synthesis of drugs and terpenic alkaloids. Though the yields of the products are low, the straightforward assembly of tri- and tetrasubstituted pyridines from simple starting materials and by a one-pot reaction is sufficiently attractive.

2.6. *m-Dichlorobenzenecarboxaldehydes*

Benzocyclisation of 1,3-diketones (**20**) by the Vilsmeier reaction methodology, leading to the formation of 2,4-dichlorobenzenecarboxaldehydes (**21**) has been realised. A phenyl substituent on the 1,3-diketone gave biphenylcarboxaldehyde.

References

1. JUTZ, C — In *Iminium salts in organic chemistry*, Part 1, 1976, pp. 225–342, (ed.) H. Bohme and H. G. Viehe, Wiley.
2. SREENIVASULU, M., SURESH CHANDER RAO, M AND KRISHNA RAO, G. S — *Indian J. Chem.*, 1987, **26B**, 173–174.
3. SREENIVASULU, M. AND KRISHNA RAO, G. S. — *Indian J. Chem.*, 1987, **26B**, 581–582
4. SREENIVASULU, M. AND KRISHNA RAO, G. S. — *Indian J Chem.*, (in press).
5. CASNATI, G , LANGELLA, M. R , PIOZZI, F., RICCA, A. AND UMANI-RONCHI, A — *Tetrahedron Lett*, 1964, 1597–1600.
6. CHEN, K. M. AND JOULLIE, M. M — *Tetrahedron Lett*, 1982, 4567–4568
7. TRAAS, P. C., BOELLENS, H AND TAKKEN, H. J — *Recl. Trav Chim. Pays-Bas.*, 1976, **95**, 308–311.
8. WOLTERSDORF, O. W JR., SOLMS, S. J., SCHULTZ, E. M. AND CRAGOE, E. J JR. — *J. Med. Chem.*, 1977, **20**, 1400–1408.
9. NEWKOME, G R. AND PAUDLER, W W. — In *Contemporary heterocyclic chemistry*, 1982, pp. 307–320, Wiley.
10. SREENIVASULU, M. AND KRISHNA RAO, G. S. — Presented at the *'Indian Chemical Society', 23rd Annual Convention of Chemists*, 1986, Abstract N. ORG (H)-10. Dec. 20–24, Annamalai University, Chidambaram.
11. JONES, G. — *Org. Reactions*, 1967, **15**, 204–599.

Thesis Abstract (Ph.D.)

High-pressure studies on germanium and gallium-based chalcogenide glasses by M. V. Narasimha Prasad.
Research supervisor: E. S. Rajagopal.
Department: Physics.

1. Introduction

Chalcogenide glassy semiconductors have become very important in recent times both scientifically and technologically. They have found extensive applications in computer memories, solar cells, xerography, holography, fibre optics, etc. It is necessary to understand the fundamental physical properties of chalcogenide glassy semiconductors in order to characterise them for device applications. The present work is concerned with the electrical resistivity measurements at high pressures and at low temperature of bulk, semiconducting, Ge_xSe_{100-x} chalcogenide glasses. Some analogous studies on the Ga_xTe_{100-x} glassy system are also reported.

2. Experimental

Bulk Ge_xSe_{100-x} glasses have been prepared in the composition range $0 \leqslant x \leqslant 45$, by the melt-quenching technique. The samples are characterised by X-ray diffraction and differential scanning calorimetry. The electrical resistivity of the glasses has been measured on a Bridgman anvil system, up to a pressure of 14 GPa. High-pressure studies at low temperatures (down to 77 K) have been performed in a continuous pressure-changing system. The details of the high-pressure systems and pressure calibration methods are discussed elsewhere[1]. A quasi-hydrostatic pressure-transmitting medium (steatite) is used in high-pressure as well as high-pressure–low-temperature experiments. A four-probe method is employed for measuring the electrical resistivity in high-pressure anvils.

A multi-range, multi-channel data logger has also been developed for the continuous acquisition of temperature and resistivity data, with a sampling interval between 20 sec and 3 min.

3. Results and discussion

The present high-pressure investigations reveal that bulk Ge_xSe_{100-x} glasses ($0 \leqslant x \leqslant 45$) exhibit a sharp, discontinuous transition in the resistivity, at high pressures. The dc conductivity measurements as a function of temperature at different pressures prior to and after the transition point indicate that the observed transition is from a semiconductor to a metal. The X-ray diffraction studies of the samples recovered from high pressures above the transition pressure, show that Ge_xSe_{100-x} glasses crystallise as and when they become metallic.

The most interesting outcome of the present investigations is the variation of the properties like the glassy semiconductor-crystalline metal transition pressure (P_T), the room temperature-atmospheric pressure resistivity (ρ_o), the glass transition temperature (T_g), etc., with composition x. The variation of P_T with x exhibits a local maximum in its value at a composition $x = 20$ and a minimum at a composition $x = 33$. Both T_g and ρ_o as a function of x, exhibit a slope change at $x = 20$ and a maximum at $x = 33$. These results indicate that the $x = 20$ and $x = 33$ compositions in Ge_xSe_{100-x} glassy system must be critical.

It has been recently proposed in the literature[2–4] that the short-range order and the physical properties of chalcogenide glasses are strongly dependent on composition. In a IV–VI chalcogenide system, glasses with very low concentrations of IV group atoms are elastically floppy, comprising predominantly under crosslinked VI group atoms. As the concentration of the IV group atoms increases, rigid molecular fragments are nucleated in the material. At $x = 20$, the rigid regions contact each other or percolate in a mean field sense[3]. Consequently, the $x = 20$ composition in IV–VI chalcogenide systems gives rise to a mechanical percolation threshold at which property anomalies can occur. The results of the high pressure investigations on Ge_xSe_{100-x} glasses provide an evidence for the existence of the mechanical critical composition.

The $x = 33$ composition in Ge_xSe_{100-x} glasses, corresponds to a chemical threshold, at which the stoichiometric crystalline compound $GeSe_2$ occurs. The present results indicate that the glasses at the chemical threshold also possess unique physical properties.

The glass-forming region in the Ga_xTe_{100-x} system is small ($15 < x < 25$). Glasses with $x = 17$, 20 and 25 have been prepared. An interesting feature of the glasses is that they exhibit the double-glass transition phenomena when heated slowly, say in a DSC run. For example, the $Ga_{20}Te_{80}$ glass has Tg_1 at 419 K and Tc_1 at 450 K. At Tc_1, excess tellurium precipitates out as crystalline fragments in an amorphous matrix. When the sample heated to Tc_1 and cooled to room temperature is heated again, it exhibits a second glass transition at $Tg_2 = 528$ K and a second crystallisation at $Tc_2 = 548$ K.

At this stage, the glassy matrix also crystallises out at Ga_2Te_3 with a zinc-blend structure. The phenomena of double-glass transition and double-stage crystallisation have been observed in many other Te-based glassy systems like Si-Te, Ge-Te, Al-Te, etc.[5-7], and are connected closely to the chemical short-range order in Te-based glasses[5,6].

The electrical resistivity measurements of Ga_xTe_{100-x} glasses show that these samples exhibit a continuous decrease in resistivity under pressure, becoming metallic around 8 GPa. The observed resistivity behaviour under pressure of Ga_xTe_{100-x} glasses is consistent with the behaviour of other III–VI chalcogenide glasses like Al_xTe_{100-x}[7].

References

1. BANDYOPADHYAY, A. K., NALINI, A. V., GOPAL, E. S. R AND SUBRAMANYAM, S. V. — *Rev. Sci. Instrum.*, 1980, **51**, 136–139.
2. PHILIPS, J. C. — *Phys. Rev. B*, 1985, **31**, 8157–8169.
3. ASOKAN, S., PARTHASARATHY, G. AND GOPAL, E. S. R. — *Phys. Rev. B*, 1987, **35**, 8269–8272.
4. ASOKAN, S., PRASAD, M. V. N., PARTHASARATHY, G. AND GOPAL, E. S. R. — *Phys. Rev. Lett*, 1989, **62**, 808–810.
5. ASOKAN, S., PARTHASARATHY, G. AND GOPAL, E. S. R. — *J. Non-cryst. Solids*, 1986, **86**, 48–64.
6. ASOKAN, S., PARTHASARATHY, G. AND GOPAL, E. S. R. — *Int. J. Rapid Solidification*, 1987, **2**, 257–271
7. PARTHASARATHY, G., RAMAKRISHNA, R., ASOKAN, S. AND GOPAL, E. S. R. — *J. Mater. Sci. Lett.*, 1986, **5**, 809–811.

Thesis Abstract (Ph.D.)

Developments in two-dimensional NMR spectroscopy of multiple quantum coherences of coupled spins in liquids by N. Murali.
Research supervisor: Anil Kumar.
Department: Physics.

1. Introduction

The advent of two-dimensional Fourier Transform NMR (2DFTNMR) spectroscopy eased the creation and detection of multiple quantum coherences (MQCs) using the principles of coherence transfer[1,2]. The MQCs contain additional information on topology of the energy level scheme of molecules in liquids. MQ spectroscopy is often used for simplification of spectral complexities and to enhance the ease of retrieval of information either by monitoring MQCs themselves through their correlation to single quantum coherences or by effecting single quantum–single quantum coherence transfer *via* MQ orders in the form of a filter. MQCs have additional information about relaxation process as their relaxation rates contain information about the power spectral densities that reveal the correlation of relaxation mechanisms acting on different nuclei.

This thesis deals with developmental work associated with MQCs in 2DNMR spectroscopy. Methods for enhancing the information content of 2D MQ experiments are analysed and a detailed study of appearance of the MQ artifacts in 2D spectra is presented. New techniques to yield pure-phase MQ filtered and longitudinal spin order-filtered correlated spectra are developed.

2. Flip angle dependences of MQCs

The three pulse MQ spectroscopy normally uses a 90° coherence transfer pulse which attempts to distribute coherences equally among various coherence transfer pathways. It is shown that a variation of the flip-angle of the mixing pulse allows distinction between various classes and types of transitions as well as optimisation of experiment for selective detection of certain classes of peaks in 2D spectra and enhances the information content. For this purpose a pathway description developed earlier for COSY is generalised to include MQ spectroscopy which facilitates the delineation of the contributions of various paths to the intensity of a peak in MQ spectroscopy. Based on this pathway description, the connectivity classes of COSY are also generalised to include MQ spectroscopy[3].

3. MQ artifacts in COSY

In this section a study of the appearance of MQ artifacts in 2D COSY experiment is described. The two-pulse COSY experiment when performed with fast repetition rates in order to optimise signal-to-noise ratio with performance time can be, in essence, considered as a three-pulse experiment. Under such circumstances MQCs are created from the non-equilibrium state of the spin system arising due to insufficient relaxation delays. Generally, in these non-equilibrium states the state of the spin system can be represented by populations, and the density matrix describing the system commutes with its Hamiltonian (non-equilibrium state of kind I). These MQCs, which are the carried-over information of such a non-equilibrium state from one experiment to another, often appear as artifacts along MQ diagonals for strongly coupled spins. These have been observed in 2D COSY spectra of several peptides and oligonucleotides. A spin-temperature picture which defines two parameters, of which one is the lack of spin temperature in the spin system, and the other the difference in spin temperature of the sub-systems formed by sets of pairs of energy levels of the spins, is developed. A detailed relaxation evolution of these parameters, based on density matrix relaxation calculations, is carried out to account for the observed MQ artifacts[4].

4. Longitudinal spin order filtering

A new pulse pair filtering technique which yields pure-phase 2D spectra in MQ-filtered COSY and other correlated experiments is described. In MQ-filtered COSY experiments when the order of filtering is less than the number of coupled spins the diagonal peaks have a mixture of absorption and dispersion line shapes. The presence of dispersive components hinders the resolution due to their broad wings while the narrow absorption component aids the resolution and thus becomes the preferred mode of presenting 2D spectrum. A 45° pulse pair filter is proposed here, which when inserted before detection in such experiments, yields a pure-phase spectrum. This pulse-pair filter is also generalised to yield pure-phase spectra in various 2D experiments. Experiments were carried out to demonstrate the use of 45° pulse-pair filter in double-quantum filtered experiment[5].

The idea of 45° pulse-pair filtering and its generalisation to yield a pure-phase 2D spectrum led to a completely new method of coherence-transfer process in COSY experiments, namely, coherence transfer *via* longitudinal spin order (CLOSY). This method which is an alternative to MQ-filtered COSY, yields pure-phase two or more spin-filtered spectra irrespective of coupling strength and

number of coupled spins. The symmetry in CLOSY is also investigated. A detailed theoretical description of CLOSY and the experimental results are also given[6].

References

1 AUE, W. P., BARTHOLDI, E. AND ERNST, R. R. — Two-dimensional spectroscopy. Application to nuclear magnetic resonance, *J. Chem. Phys.*, 1976, **64**, 2229–2248

2 ERNST, R. R., BODENHAUSEN, G. AND WOKAUN, A. — *Principles of nuclear magnetic resonance in one and two dimensions*, 1987, Clarendon Press.

3. MURALI, N., RAMAKRISHNA, Y. V. S., CHANDRASEKHAR, K., THOMAS, M. A AND ANIL KUMAR — Flip angle dependence in two-dimensional multiple quantum coherence NMR spectroscopy, *Pramana*, 1984, **23**, 547–557.

4. MURALI, N. AND ANIL KUMAR — Multiple-quantum artifacts in single-quantum two-dimensional correlated NMR spectra of strongly coupled spins, *Chem. Phys. Lett.*, 1986, **128**, 58–61.

5 MURALI, N., CHANDRASEKHAR, K AND ANIL KUMAR — Use of 45° pulse pair as a filter for pure-phase two-dimensional NMR spectroscopy, *J. Magn. Resonance*, 1986, **70**, 153–156.

6 MURALI, N. AND ANIL KUMAR — Coherence transfer *via* longitudinal spin order and generalized pulse pair for pure-phase two-dimensional NMR spectroscopy, *Chem. Phys. Lett.*, 1987, **137**, 324–329.

Thesis Abstract (Ph.D.)

Studies of some interfacial properties in a critical binary liquid system by Sabyasachi Guha.
Research supervisor: E. S. R. Gopal.
Department: Physics.

1. Introduction

The mutual solubility of a partially miscible binary liquid mixture is generally represented by the coexisting curve in a temperature-concentration plane. The highest phase separation temperature as obtained by the coexistence curve is the critical temperature (T_c) and the corresponding concentration is the critical concentration. Below the critical temperature the mixture exhibits two distinct phases separated by a meniscus. On approaching T_c the distinction between the phases disappears and various thermodynamic quantities vanish or diverge at a critical point proportional to some power of the distance, often measured as $(T_c - T)$, from the point[1,2].

Like many other quantities the interfacial tension σ between the coexisting phases vanishes on approaching T_c with a power law,

$$\sigma = \sigma_0(-t)^{\mu} \tag{1}$$

where $t = (T - T_c)/T_c$ and μ is the critical exponent for surface tension. This exponent is estimated experimentally for the system cyclohexane-acetonitrile. The particular system has been chosen because of its very low-gravity affected region.

The vanishing interfacial tension leads to the very interesting critical point wetting phenomenon.

In critical point wetting, the liquid vapour and the liquid-solid interfaces should be completely wetted by one of the components near the critical point. In the present system, the heavier cyclohexane-rich phase resides at the liquid vapour interface on the top of the acetonitrile-rich phase. This induces Rayleigh-Taylor interface instability[3-5]. The condition for a stable wetting layer is obtained and the result is verified qualitatively.

The wetting behaviour of the system is studied in a simulated micro-g environment. The micro-g environment is simulated by adding a dopant *e.g.* water and acetic anhydride. The effect of impurity on the critical temperature is also determined.

2. Experimental

The cyclohexane and acetonitrile were of analytical reagent grade. They were further purified by distilling cyclohexane over lithium aluminium hydride and acetonitrile over molecular sieves. The liquids were then kept in a glove box under a dry nitrogen atmosphere. They were degassed before use.

The interfacial tension was measured by the capillary rise method. The position of the interface in a cylindrical capillary tube is observed. The height difference h between the cell interface and the capillary interface is converted to a^2 through the equation

$$a^2 = r(h + r/3 - 0.1288r^2/h + 0.1312r^3/h^2) \tag{2}$$

which in turn is related to the surface tension σ by

$$\sigma = (a^2 g \Delta\rho)/2 \tag{3}$$

where $\Delta\rho$ is the density difference between the coexisting phases and g the acceleration due to gravity.

The experiment was carried out in a paraffin oil bath of capacity 10 litres. The temperature of the well-stirred liquid bath was controlled to 1 mK. The temperature was measured by a platinum resistance thermometer which has a resolution of 0.1 mK. The height difference of the meniscus was measured by a cathetometer that can be read to ± 0.001 cm.

The vertical distance between the interfaces in the capillary and the cell was measured as a function of temperature. The observed capillary rise was converted to the capillary parameter a^2 assuming that the contact angle remained zero close to T_c. The density difference between the coexisting phases in equilibrium near the critical point was calculated from the measurements of the coexisting compositions measured as volume fraction[6]. Using this density difference, the interfacial tension was calculated from eqn (2) and fitted to a power law in the temperature range $5 \times 10^{-4} < t < 5 \times 10^{-3}$. Log-log plot of σ *vs* $(T_c - T)$ is shown in fig. 1. This fit gave a value of $\mu = 1.26 \pm 0.02$ and $\sigma_0 = 97.8$ dynes/cm where the parameters are defined in eqn (1).

The interfacial tension of a water (0.01 w.f. of acetonitrile)-doped cyclohexane–acetonitrile mixture was also measured. The parameters of eqn (1) obtained in this measurement were $\mu = 1.29 \pm 0.02$ and $\sigma_0 = 69.8$ dynes/cm.

Using the values of the experimentally determined capillary parameter, the Rayleigh-Taylor instability of the wetting layer was verified qualitatively. The limit of the stability was calculated by using the condition for a stable wetting layer

$$R^2 < (4\sigma_0/g\Delta\rho)(T_c - T)^{\mu} \tag{4}$$

where R is the radius of the experimental cell. The wetting layer was found to be stable in a cell of diameter 1 cm when the temperature was more than 2.5°C away from T_c, whereas, at the same

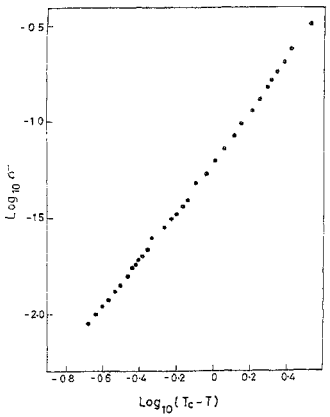

FIG. 1. Log-log plot of interfacial tension *vs* $(T_c - T)$.

temperature, in a bigger cell, the wetting layer was unstable. Due to the onset of the instability in a bigger cell the single wetting layer broke into smaller drops.

A preliminary study of the wetting behaviour and the phase separation in simulated micro-g environment was made. The densities and the thermal expansion coefficients of the components *i.e.* cyclohexane and acetonitrile were such ($\rho_A = 0.782$ g/cc and $\rho_C = 0.780$ g/cc at 20°C; $\alpha_A = 0.00138$/°C and $\alpha_C = 0.00120$/°C) that there was a density inversion (T_i) at 31°C. Close to the inversion temperature, measurement of capillary parameter was specially difficult; even in a tube of 1 cm diameter the interfacial meniscus rose about 5 cm. Therefore, the capillary parameter was measured in a range from T_i to T_c. This parameter is needed to measure the angle of contact from the meniscus profile. The micro-g environment was simulated by bringing T_i as close as possible to T_c. This was achieved by adding a dopant *e.g.* water and acetic anhydride. The change in T_c and T_i with impurity concentration was measured. In the case of water $dT_c/dX \sim 3.7 \times 10^{-1}$ K/0.1 wt% of H_2O in CH_3CN and $dT_i/dX \sim 1.7$ K/0.1 wt% of H_2O in CH_3CN. In the case of acetic anhydride $dT_c/dX \sim -2.0 \times 10^{-3}$ K/0.1 wt% of $C_4H_6O_3$ in CH_3CN and $dT_i/dX \sim 9.1 \times 10^{-1}$ K/0.1 wt% of $C_4H_6O_3$ in CH_3CN. Therefore, at about 4.5 wt% of $C_4H_6O_3$ in CH_3CN the $T_i \approx T_c \approx 75$°C and the phase separation occurred in micro-g environment.

References

1. STANELY, H. E. *Introduction to phase transition and critical phenomena*, 1971, Oxford University Press.

2. KUMAR, A., KRISHNAMURTHY, H. R. AND GOPAL, E. S. R. Equilibrium critical phenomena in binary liquid mixture, *Phys. Rep.*, 1983, **98**, 57–143.

3 TAYLOR, G.	The instability of liquid surfaces when accelerated in a direction perpendicular to their planes. I, *Proc. R. Soc.*, 1950, **201A**, 192–209.
4. CHANDRASEKHAR, S.	*Hydrodynamic and hydromagnetic stability*, 1961, Ch. X, Clarendon Press.
5. CHATTERJEE, S., VANI, V., GUHA, S. AND GOPAL, E. S. R.	Critical wetting phenomena: Observation of hydrodynamic instabilities, *J. Phys.*, 1985, **46**, 1533–1541.
6. VANI, V., GUHA, S. AND GOPAL, E. S. R.	Coexistence curve of acetonitrile and cyclohexane liquid system, *J. Chem. Phys.*, 1986, **84**, 3999–4007.

Thesis Abstract (Ph.D.)

Transient capacitance studies of some deep levels in silicon by H. Indusekhar.
Research supervisor: Vikram Kumar.
Department: Physics.

1. Introduction

Deep impurity levels play an important role in controlling electrical and optical properties of semiconductor devices. Hence it is necessary to characterise[1] these impurities to know their physical behaviour and to understand solid-state phenomena. However, the understanding of deep levels is poor compared to their counterparts, namely, the shallow levels. Deep levels are created in silicon either by irradiation with high-energy particles or by the addition of impurities other than from group three and five of the periodic table. Deep impurities are characterised by large ionisation energies, multiple-charge states and fast-diffusion coefficients. Space-charge transient techniques[2], in particular DLTS, are used in the present work to investigate the properties of deep levels introduced in silicon due to processing at high temperature, irradiation with high energy, high-dose alpha particles and intentional contamination of nickel.

2. Results and conclusions

Two deep levels are noticed[3] in *p*-silicon due to processing at high temperature. These levels are related to iron by earlier workers. The sources of iron contamination are investigated and found to be ambient conditions, in particular age of quartz tube. The two levels are located at $E_v + 0.42$ eV and $E_v + 0.52$ eV as determined by TSCAP, DLTS and photo-capacitance methods. The photoionisation cross-sections[4] are well described by Lucovsky's model. The identical optical and thermal ionisation energies of the two levels imply near-zero lattice relaxation. The hole capture by $E_v + 0.42$ eV level is thermally activated with a barrier of 40 meV. The two levels are stable contrary to a few earlier reports. The conflicting reports about the stability and the variation in the reported capture cross-section values of thermally induced level at $E_v + 0.4$ eV suggests that $E_v + 0.42$ eV level must be a complex centre and not just interstitial iron.

Irradiation of *n*-silicon with alpha particles of 30 MeV energy at a dose of 10^{14} and 10^{15} cm^{-2} has induced five deep levels. The radiation related levels[5] at $E_c - 0.18$ eV, $E_c - 0.26$ eV and $E_c - 0.48$ eV are identified as A centre, double and single negatively charged divacancy, by comparing their electrical properties and annealing behaviour with that reported for these defect complexes. Two other levels, at $E_c - 0.28$ and $E_c - 0.51$ eV, could not be related to any known centre.

Intentional contamination of n- and p-silicon with nickel[6] at high temperatures shows that nickle introduces deep levels only in the lower half of the band gap. Five deep levels are observed at $E_v + 0.15$, $E_v + 0.18$, $E_v + 0.32$, $E_v + 0.15$ and $E_v + 0.54$ eV in the electroless-plated nickel-diffused samples. The level at $E_c + 0.15$ and $E_c + 0.54$ eV is not related to nickel since they are absent in the evaporated nickel-diffused samples. The concentration of these levels is dependent on the quenching mode. The enthalpy of formation, observed annealing behaviour at both room and high temperatures as well as stability of the main nickel-related level at $E_v + 0.32$ eV in the packaged samples are explained by suggesting that this centre is a nickel vacancy complex, the concentration of which has a definite ratio with the total interstitial nickel concentration.

References

1. CHEN, J. W. AND MILNES, A. G. *Annu. Rev Mater. Sci.*, 1980, **10**, 157–228.
2. GRIMMEISS, H G. *Annu. Rev. Mater. Sci.*, 1977, 7, 341–376.
3 INDUSEKHAR, H. AND KUMAR, V. *Physica Stat. Sol. (a)*, 1986, **95**, 269–278.
4. INDUSEKHAR, H. AND KUMAR, V. *J. Phys. C-Solid St. Phys.*, 1985, **18**, 5095–5098.
5. INDUSEKHAR, H, SENGUPTA, D. AND KUMAR, V. *Physica Stat. Sol. (a)*, 1986, **93**, 645–653.
6. INDUSEKHAR, H. AND KUMAR, V. *J. Appl. Phys.*, 1987, **61**, 1449–1455.